



HAL
open science

Optical properties of epitaxial $\text{Na}_{0.5}\text{Bi}_{0.5}\text{TiO}_3$ lead-free piezoelectric thin films: Ellipsometric and theoretical studies

Krzysztof Dorywalski, Nathalie Lemee, Bohdan Andriyevsky, Ruediger Schmidt-Grund, Marius Grundmann, Michal Piasecki, Marie Bousquet, Tomasz Krzyzynski

► To cite this version:

Krzysztof Dorywalski, Nathalie Lemee, Bohdan Andriyevsky, Ruediger Schmidt-Grund, Marius Grundmann, et al.. Optical properties of epitaxial $\text{Na}_{0.5}\text{Bi}_{0.5}\text{TiO}_3$ lead-free piezoelectric thin films: Ellipsometric and theoretical studies. *Applied Surface Science*, 2017, 421 (B, SI), pp.367-372. 10.1016/j.apsusc.2016.09.078 . hal-03628160

HAL Id: hal-03628160

<https://u-picardie.hal.science/hal-03628160>

Submitted on 5 Sep 2023

HAL is a multi-disciplinary open access archive for the deposit and dissemination of scientific research documents, whether they are published or not. The documents may come from teaching and research institutions in France or abroad, or from public or private research centers.

L'archive ouverte pluridisciplinaire **HAL**, est destinée au dépôt et à la diffusion de documents scientifiques de niveau recherche, publiés ou non, émanant des établissements d'enseignement et de recherche français ou étrangers, des laboratoires publics ou privés.

Accepted Manuscript

Title: Optical properties of epitaxial $\text{Na}_{0.5}\text{Bi}_{0.5}\text{TiO}_3$ lead-free piezoelectric thin films: ellipsometric and theoretical studies

Author: Krzysztof Dorywalski Nathalie Lemée Bohdan Andriyevsky Rüdiger Schmidt-Grund Marius Grundmann Michał Piasecki Marie Bousquet Tomasz Krzyżyński



PII: S0169-4332(16)31947-X
DOI: <http://dx.doi.org/doi:10.1016/j.apsusc.2016.09.078>
Reference: APSUSC 34007

To appear in: *APSUSC*

Received date: 29-7-2016
Accepted date: 17-9-2016

Please cite this article as: Krzysztof Dorywalski, Nathalie Lemée, Bohdan Andriyevsky, Rüdiger Schmidt-Grund, Marius Grundmann, Michał Piasecki, Marie Bousquet, Tomasz Krzyżyński, Optical properties of epitaxial $\text{Na}_{0.5}\text{Bi}_{0.5}\text{TiO}_3$ lead-free piezoelectric thin films: ellipsometric and theoretical studies, *Applied Surface Science* <http://dx.doi.org/10.1016/j.apsusc.2016.09.078>

This is a PDF file of an unedited manuscript that has been accepted for publication. As a service to our customers we are providing this early version of the manuscript. The manuscript will undergo copyediting, typesetting, and review of the resulting proof before it is published in its final form. Please note that during the production process errors may be discovered which could affect the content, and all legal disclaimers that apply to the journal pertain.

Optical properties of epitaxial $\text{Na}_{0.5}\text{Bi}_{0.5}\text{TiO}_3$ lead-free piezoelectric thin films: ellipsometric and theoretical studies

Krzysztof Dorywalski ^{1*}, Nathalie Lemée ², Bohdan Andriyevsky ³, Rüdiger Schmidt-Grund ⁴, Marius Grundmann ⁴, Michał Piasecki ⁵, Marie Bousquet ², Tomasz Krzyżyński ¹

¹ Faculty of Technology and Education, Koszalin University of Technology, Śniadeckich Str. 2, PL-75-453 Koszalin, Poland

² Laboratory of Condensed Matter Physics, EA 2081, University of Picardie Jules Verne, 33 rue Saint-Leu, 80039 Amiens Cedex 1, France

³ Faculty of Electronics and Computer Sciences, Koszalin University of Technology, Śniadeckich Str. 2, PL-75-453 Koszalin, Poland

⁴ Universität Leipzig, Fakultät für Physik und Geowissenschaften, Institut für Experimentelle Physik II, Linnéstr. 5, 04103 Leipzig, Germany

⁵ Institute of Physics, J. Długosz University, Al. Armii Krajowej 13/15, PL-42-200 Częstochowa, Poland

* krzysztof.dorywalski@tu.koszalin.pl

Highlights:

- Ultra-thin $\text{Na}_{0.5}\text{Bi}_{0.5}\text{TiO}_3$ films were epitaxially deposited on (001) SrTiO_3 substrate by pulsed laser deposition
- Real and imaginary parts of the complex dielectric function were determined
- The electronic transitions related to the fundamental absorption edge are of indirect type
- Phonons involved in the band gap transition can be primarily associated with vibrations involving oxygen atoms
- Electronic transitions in the VUV comes from the O $2p$ valence band levels to Ti $3d$ conduction band levels and a little to the Bi p levels

Abstract

Ultra-thin $\text{Na}_{0.5}\text{Bi}_{0.5}\text{TiO}_3$ films were epitaxially deposited on (001) SrTiO_3 substrate by pulsed laser deposition. From the ellipsometric spectra collected in the photon energy range 2–8.7 eV, real and imaginary parts of the complex dielectric function were determined. It was found, that the electronic transitions related to the fundamental absorption edge are of indirect type, which is confirmed by *ab initio* band structure calculations. This finding is in contradiction to previous theoretical studies but in agreement with the most recent experimental works. Based on their determined energies, phonons involved in the band gap transition can be primarily associated with vibrations involving oxygen atoms. Main contributions to the VUV absorption spectra come from the electronic transitions from the O $2p$ valence band levels to Ti $3d$ conduction band levels and a little to the Bi p levels.

keywords: NBT, $\text{Na}_{0.5}\text{Bi}_{0.5}\text{TiO}_3$, dielectric function, refractive index, thin film, band structure

1. Introduction

Piezoelectric materials are widespread used in today's sensor, actuator and transducer devices. However, the most common ones, like lead zirconate titanates $\text{Pb}(\text{Zr}_x\text{Ti}_{1-x})\text{O}_3$ (PZT), contain relatively high amount of lead (60% Pb by weight in case of PZT). Due to its harmful effect, the usage of lead and other hazardous elements has been limited by regulations. This implies strong efforts in the developing of less hazardous, alternative lead-free piezoelectric materials in recent years.

Sodium bismuth titanate $\text{Na}_{0.5}\text{Bi}_{0.5}\text{TiO}_3$ (NBT) is considered to be one of the most promising lead-free piezoelectric, susceptible to replace PZT. It has a relatively large remnant polarization ($P_r = 38 \mu\text{C}/\text{cm}^2$), high Curie temperature of $320 \text{ }^\circ\text{C}$ and coercive field $E_c = 73 \text{ kV}/\text{cm}$ [1, 2]. Since its discovery in 1961 [1], the electrical properties of NBT were extensively studied, unlike optical properties of NBT in the diverse form, which are rather scarce. Such data are essential not only for theoretical studies of phase transition mechanisms and the nature of electronic transitions, but also for possible optoelectronic applications of NBT.

The pseudo-dielectric function in the wide spectral range 2–9.5 eV of a NBT single crystal was reported by Andriyevsky *et al.* [3], determined by means of spectroscopic ellipsometry using synchrotron radiation as a light source. They, however, did not take into account surface imperfection during the ellipsometric data analysis, causing pronounced non-zero values of the imaginary part of the dielectric permittivity in the crystal's transparency spectral range in their study. Therefore, although the overall lineshape of the presented optical spectra seems to be reasonable, the exact values of the real and imaginary part of the complex dielectric function (DF) cannot be used as a reference. Previously, only UV-visible absorption spectra on pure and Mn-doped NBT crystals were reported [4]. Regarding NBT thin films, near-band gap optical spectra were determined by Kim *et al.* for a NBT film synthesized by the sol-gel method [5], and Bousquet *et al.* for NBT grown on MgO by laser ablation [6]. Both works claim indirect character of the optical band gap, which is either in contradiction [7] or find no confirmation [8] in previous theoretical studies of the electronic structure of NBT.

In this work, we focus on the optical properties of epitaxial NBT thin films grown on SrTiO_3 (STO) substrates in the spectral ranges of the material's transparency and fundamental absorption using both, experimental (ellipsometric) and theoretical (*ab initio* calculations) approaches.

2. Experimental

2.1 Samples

Two samples of NBT thin films, denoted as NBT1 and NBT2, were grown on SrTiO₃ (001) substrate by Pulsed Laser Deposition (PLD), using a KrF excimer laser ($\lambda = 248$ nm, pulse duration = 20 ns). The ceramic targets for PLD with nominal composition Na_{0.55}Bi_{0.55}TiO₃ were produced in a two-step process by a conventional ceramic route (relative density up 90% for NBT). The excess in bismuth and sodium aims to compensate the losses during the deposition process. The thin films were grown using a laser fluence around 2–3 J/cm² and a pulse rate of 2 Hz. The deposition temperature (T_{dep}) and the oxygen partial pressure (PO₂) were $T_{\text{dep}} = 650$ °C and PO₂ = 0.4 mbar for the two samples. During the growth, the number of pulses for the NBT1 sample was 500 and for NBT2 1500. The surface quality of the layers was analyzed by Reflection High-Energy Electron Diffraction (RHEED). Standard θ -2 θ X-Ray Diffraction (XRD) patterns and ω -scans were recorded using a Siemens D5000 diffractometer with Cu K α_1 radiation.

2.2 Ellipsometry

Spectra of the ellipsometric parameters $\Psi(E)$ and $\Delta(E)$ were recorded in the wide photon energy range of $E = 2$ –8.7 eV using a Woollam VUV-VASE ellipsometer, and additionally a VASE ellipsometer in the range up to 5 eV. The spectra were evaluated by transfer matrix calculations within a layered optical model being STO substrate/NBT film/surface imperfection. The optical constants for the STO substrate were taken from our previous study [9]. The roughness of the surface was approximated by effective medium theory (effective medium approximation EMA) according to Bruggeman [10], assuming 50% of voids in the matrix of NBT. Since the NBT crystal structure can be described as pseudo-cubic ($\alpha = 89.8^\circ$) [11] and furthermore the c -axis of the film is oriented perpendicular to the surface plane, it was no need to take into account optical anisotropy during data modeling. This was confirmed by measuring of Muller matrix elements [12], where the off-diagonal ones are found to be equal to zero, what additionally shows absence of any strain induced anisotropy.

2.3 Calculations

Calculations of the band structure (BS) and optical properties of the materials studied have been performed by the CASTEP program [13], based on the density functional theory (DFT) and plane-waves, using the ultrasoft pseudopotentials [14]. The generalized gradient

approximation (GGA) for the exchange and correlation effects [15] and the cutoff energy 370 eV for the plane-waves basis set were used. During self-consistent electronic minimization, the eigen-energy convergence tolerance was chosen to be $1.0 \cdot 10^{-6}$ eV and the tolerance for the electronic total energy convergence during optimization was $1 \cdot 10^{-5}$ eV. Also, the corresponding maximum ionic force tolerance was $3 \cdot 10^{-2}$ eV/Å, the maximum stress component tolerance was taken to be $5 \cdot 10^{-2}$ GPa and the maximum atomic displacement was 0.001 Å. Optimization (relaxation) of the atomic positions and crystal's unit cell parameters were performed for all samples studied.

The BS and dielectric function $\varepsilon(\hbar\omega)$ of bulk NBT were calculated for the optimized crystal structure at the hexagonal crystal unit cell (space group $R3$, no. 146) of the dimensions $a = b = 5.50$ Å, $c = 13.87$ Å, $V = 363.7$ Å³, at 25 irreducible k -points (the k -points grid $5 \times 5 \times 2$). The unit cell of the bulk NBT contains 6 formula units. Because the relatively thin NBT films on SrTiO₃ (001) substrates were studied here by spectroscopic ellipsometry, the corresponding calculations of dielectric function, to be adequate enough to the experimental one, should take into account the NBT surface electronic states (1) and the atomic reconstruction of NBT surface layers (2). These effects may influence the dielectric function of NBT films studied. Therefore, we have calculated also BS and dielectric function of the supercell comprising the NBT slab and the vacuum gap. The NBT slab is infinite in the X - and Y -directions and is of the finite thickness in the perpendicular Z -direction. Thicknesses of this slab were taken to be one, two, and four unit cell dimensions of NBT single crystals along Z -direction. The thickness of the vacuum gap of the supercell in Z -direction was taken to be 10 Å to avoid interatomic interaction between the neighboring NBT slabs. The optimized space group symmetry of all samples of NBT slabs studied was found to be $P3$ (no. 143). The dielectric functions of the NBT slabs were calculated at 13 irreducible k -points (the k -points grid $5 \times 5 \times 1$).

3. Results and discussion

Figure 1 shows the RHEED patterns observed for the STO substrate as well as the NBT1 and NBT2 thin film samples. As reported in a previous paper [16], the spatial coincidence of the RHEED 001-azimuth-pattern of the films and the substrate indicate a cube-on-cube epitaxial growth. The RHEED patterns consist of broad asymmetric spots superposed on the streaks,

pointing out a possible transition of the epitaxial growth from 2D nucleation to 3D nucleation. For NBT2, the spots are broader indicating a rougher surface in this thicker sample.

NBT is a rhombohedral or monoclinic perovskite [17] at room temperature, but the associated pseudo-cubic unit cell is characterized by a lattice parameter $a_{pc\ NBT} = 3.89\ \text{\AA}$, and an angle $\alpha_{pc} = 89.8^\circ$. Considering the lattice parameter of the cubic STO substrate $a_{STO} = 3.905\ \text{\AA}$, the lattice mismatch at room temperature between STO and NBT is about +0.4 %. Figure 2 presents the out-of-plane XRD profile of NBT1 and NBT2. No secondary phases were detected within the detection limits of the diffractometer. The thin films exhibit a highly oriented (001) perovskite phase since only (00 l) peaks are observed. The out-of-plane lattice parameter, calculated from the (002) reflexes, for the NBT1 and NBT2 films are 3.85 \AA and 3.86 \AA , respectively. These lattice constants are a little smaller than that of the bulk, as a result of the tensile strain induced by the epitaxial strain on STO. Using Scherrer's relation, we have estimated the average grain size of the films from the Full Width at Half Maximum (FWHM) of the (002) diffraction peaks. We have determined values of 35.5 nm for NBT1 and 14.5 nm for NBT2.

The full width at half maximum (FWHM) value of the rocking curve around the (002) diffraction peak (Fig. 3) is 0.3° for the thin sample (NBT1) and 0.4° for the thicker one (NBT2). These values are close to that of the SrTiO₃ substrate (FWHM = 0.3°), indicating a good crystallinity and a good coherency.

The calculated band gap of bulk NBT is $E_g = 2.81\ \text{eV}$ and is found to correspond to an indirect transition (Fig. 4). The band's energy dispersion $E(k)$ is moderate for the valence bands in the range -5 eV - 0 eV and for the upper group of the conduction bands (4.8–9.0 eV), whereas it is rather small for the lowest conduction bands in the range 2.8–4.0 eV.

Comparing the atomic level resolved partial density of states (PDOS) for the samples studied, we have found that the energy width of the upper group of valence bands of the NBT slabs is larger than for the bulk material, 7 eV vs. 5 eV, correspondingly (Fig. 5). This is caused by

the fact that the smaller the slab thickness is, the smaller is the hybridization of electronic states. The latter leads to the shrinking of the energy width of the hybridized bands (Fig. 5a). Main contributions to the valence-to-conduction bands transitions come from the electronic charge transfer from the O $2p$ valence band levels to Ti $3d$ conduction band levels and a little to the Bi p levels (Fig. 5).

Because the calculated value of dielectric permittivity ε is directly proportional to the number of electronic states (and therefore to the number of atoms in the NBT slab), and is inversely proportional to the supercell volume, we have normalized the imaginary part of the calculated DF $\varepsilon_2(E)$ of the NBT supercells to the corresponding volumes of the slab without the empty space of the NBT supercell, denoted as $\varepsilon_2^{(V)}(\hbar\omega)$ (Fig. 6). The corresponding real parts $\varepsilon_1^{(V)}$ are presented in Fig. 6 (left panels).

The experimental ellipsometric spectra of both thin film samples are shown in Figure 7 (dots). From model approximation using the classical Cauchy dispersion formula [12] in the spectral range of material's transparency (400–600 nm; 2–3 eV), we have extracted the thicknesses of the NBT films as 15.37 nm and 44.94 nm for NBT1 and NBT2, respectively, the thicknesses of the surface roughness layers (2.88 and 2.19 for NBT1 and NBT2, respectively) as well as their refractive index dispersion (Fig. 8). The obtained layer thicknesses are similar to those estimated from the x-ray diffraction intensity (14.5 nm and 35 nm). One can observe increasing values of the refractive index with the increase of the film thickness, namely, at a fixed wavelength of 500 nm, $n=2.44$, 2.48, and about 2.56 [6] / 2.55 [3] for 15.37 nm, 44.57 nm and 369.8 nm film thickness and the bulk, respectively. The value of the refractive index for bulk NBT of work [3] is smaller than expected, which is undoubtedly due to the influence of surface imperfection on the pseudo-refractive index, and the real values are most likely substantially greater. Cross-check of the surface properties by atomic force microscopy tomography scans reveals good agreement of the obtained *rms* values with the determined EMA layer thicknesses. In the next step, the ellipsometric spectra were numerically approximated point-by-point in the whole spectral range while keeping the above determined layer thicknesses, and the real and imaginary parts of the complex dielectric functions were extracted.

We described the obtained DF by a line-shape model consisting of a set of Gaussian oscillators in the high-absorption spectral range and, for the near-band gap range, a Cody-Lorentz (C-L) oscillator [18]. The results of the approximation of this parametric model DF to the numerically obtained ones are shown in Fig. 8 (solid lines). A good agreement between both is obtained. The resulted DFs are shown in Fig. 9 and the parameters of the oscillators are presented in Tabs. 1 and 2. The spectra match very well with those obtained from our *ab initio* calculations (Fig. 6). The imaginary part of the DF is dominated by two broad absorption peaks centered at about 4.7 eV and 7.2 eV. A distinct shoulder in the low-energy side of the main peak of $\varepsilon_2(E)$ can be observed for the thicker layer which is impressed upon additional Gaussian oscillator centered at 3.95 eV. According to the band structure calculations, main contributions to the VUV absorption come from the electronic transitions from the O $2p$ valence band levels to Ti $3d$ conduction band levels and little to the Bi p levels [6] (see Fig. 5).

To characterize the optical band gap properties, we used Tauc relation [19]:

$$\alpha E \propto A(E - E_g)^n \quad (1)$$

where A is a constant representing the oscillator strength, $E = \hbar\nu$ the photon energy, E_g is the allowed energy gap and n is an exponent determined by the nature of the electronic transition ($1/2$ and 2 for allowed direct and indirect transition, respectively), and $\alpha = 4\pi k/\lambda$ is the absorption coefficient. For the indirect inter-band optical transitions the absorption coefficient reads [19]

$$\alpha E \propto \begin{cases} A(E - E_g^{(i)\pm})^2, & \text{for } E \geq E_g^{(i)\pm} = E_g^{(i)} \pm \hbar\Omega \\ 0, & \text{otherwise} \end{cases} \quad (2)$$

where $E_g^{(i)}$ is the indirect band gap energy and $\hbar\Omega$ is the energy of the absorbed (+) or emitted (-) phonons [19]. From equation (2), it follows that a plot of $(\alpha E)^{1/2}$ versus the photon energy E should show two linear parts around the band gap. Indeed, this is the case when looking on the $(\alpha E)^{1/2} \sim E$ plot for the NBT films (Fig. 11, squares), where two adjoining regions of linear-like dependences can be identified. As the photon energy increases, the onset of absorption near the band edge related to the indirect band-band transition starts at a photon

energy of $E^- = E_g^{(i)} - \hbar\Omega$ along with phonon absorption. When the photon energy reaches $E^+ = E_g^{(i)} + \hbar\Omega$, the photon absorption occurs along with the creation of phonons of energy $\hbar\Omega$. The values of E^- , E^+ and $E_g^{(i)}$ can be determined from the interceptions of the corresponding straight lines fittings with the energy axis ($\alpha = 0$).

The difference $1/2(E^+ - E^-)$ is found to be about 50 meV and 40 meV, which corresponds to the characteristic phonon energie $\hbar\Omega \approx 400 \text{ cm}^{-1}$ and 320 cm^{-1} for NBT1 and NBT2, respectively. Comparing these values to recent calculations of the lattice dynamics in NBT [20], the energies of the phonons involved in the indirect band gap transitions can be primarily associated with vibrations of the oxygen atoms. The determined energy of the indirect gap $E_g^{(i)}$ is about 3.36 eV and 3.44 eV for NBT1 and NBT2, respectively, with the accuracy of ± 0.02 eV. These values are close to that determined by the parametrized Cody-Lorentz dispersion model applied to the numerical $\epsilon_2(E)$ data (see table 2). The energies of the indirect band gap determined here are very similar to that obtained for an 369.8 nm thick NBT film grown on MgO as determined from optical transmission data (3.30 eV), diffused reflectance data (3.26 eV), and ellipsometry by fitting the Tauc-Lorentz oscillator directly to the ellipsometric spectra (3.18 eV) [6], as well as to that of a sol-gel grown 700 nm thick NBT [5] (3.0 eV), and to values reported for $(\text{Na}_{1-x}\text{K}_x)_{0.5}\text{Bi}_{0.5}\text{TiO}_3$ (3.45-3.48) [21].

The direct bad gap energy $E_g^{(d)}$ is obtained from the linear dependence $(\alpha E)^2 \sim E$ (figure 11, circles) to be 4.16 eV and 4.13 eV for NBT1 and NBT2, respectively, which is significantly higher than the indirect one. This supports the indirect nature of the electronic transitions processes at the band gap which is also confirmed by our *ab initio* calculations, where the indirect nature of the band structure of NBT is clearly revealed (Fig. 4).

Additionally we found a linear range in the logarithmic dependence of the absorption coefficient on the photon energy near the optical band edge (figure 11b, inset), which indicates an disorder induced exponential absorption tail known as Urbach tail [20-23],

$$\alpha = \alpha_0 \exp[\sigma(E - E_0)/k_B T] \quad (3)$$

where α_0 and E_0 are characteristic parameters of the material, σ is the steepness parameter, k_B is the Boltzmann constant, and T is the temperature. The term $k_B T/\sigma$ is known as the band tail width (Urbach tail) E_U of the localized states in the optical energy gap and can be obtained from the slope of the linear part of $\ln(\alpha) \sim E$. We found E_U to be 180 meV and 117 meV for NBT130 and NBT151, respectively, similar to the values obtained from the Cody-Lorentz model (about 200 meV).

Conclusions

The optical properties in the UV–VUV spectral range of epitaxially grown ultra-thin NBT films deposited on (001)-SrTiO₃ were studied theoretically and experimentally. Dominant features in the spectra of the dielectric function have been associated with electronic transitions from the O 2*p* valence band levels to Ti 3*d* conduction band levels. The band gap was found to be indirect and energies of the phonons involved in the indirect transitions have been obtained. The experimentally and theoretically derived results generally agree very well with each other.

References

- [1] G.A. Smolenski, V.A. Isupow, A.I. Agranovskaya, N.N. Krainik, *Sov. Phys. Solid State* 2, 2651 (1961)
- [2] J. Suchanicz, W.S. Ptak, *Ferroelectr. Lett. Sect.* 12, 71 (1990)
- [3] B. Andriyevsky, J. Suchanicz, C. Cobet, A. Patryn, N. Esser, B. Kosturek, *Phase Transitions* 82, 567 (2009)
- [4] W. Ge, H. Liu, X. Zhao, W. Zhong, X. Pan, T. He, D. Lin, H. Xu, X. Jiang, H. Luo. J, *Alloys Compd.* 462, 256 (2008).
- [5] C.-Y. Kim, T. Sekino, K. Niihara, *J. Sol-Gel Sci. Technol.* 55, 306 (2010)
- [6] M. Bousquet, J.-R. Duclere, E. Orhan, A. Bouille, C. Bachelet, C. Champeaux, *J. Appl. Phys.* 107, 104107 (2010).
- [7] Y.-N. Xu, W.Y. Ching, *Philos. Mag.* B 80, 1141 (2000)
- [8] R. Bujakiewicz-Koronska, Y. Natanzon, *Phase Transitions* 81, 1117 (2008)
- [9] K. Dorywalski, B. Andriyevsky, M. Piasecki, N. Lemee, A. Patryn, C. Cobet, N. Esser, *J. Appl. Phys.* 114, 043513 (2013)
- [10]. D.A.G. Bruggeman, *Ann. Phys. (Leipzig)* 24, 636 (1935)
- [11] G.O. Jones, P.A. Thomas, *Acta Crystallogr., Sect. B: Struct. Sci.* 58, 168 (2002)

- [12] H. Fujiwara. Spectroscopic Ellipsometry, Principles and Application, John Wiley & Sons Ltd, 2007.
- [13] S.J. Clark, M.D. Segall, C.J. Pickard, P.J. Hasnip, M.J. Probert, K. Refson, M.C. Payne, *Zeitschrift für Kristallographie* 220, 567 (2005)
- [14] D. Vanderbilt, *Phys. Rev. B* 41, 7892 (1990)
- [15] J.P. Perdew, K. Burke, M. Ernzerhof, *Phys. Rev. Lett.* 77, 3865 (1996)
- [16] M. Bousquet, L. Batista, J. L. Dellis, A. Boule, U. Rabe, O. Durand-Drouhin, Y. Gagou, L. Dupont, V. Viallet, A. Zeinert, S. Hirsekorn, N. Lemée, *J. Appl. Phys.* 116, 194104 (2014)
- [17] E. Aksel, J.S. Forrester, J.L. Jones, P.A. Thomas, K. Page, M.R. Suchomel, *Appl. Phys. Lett.* 98, 152901 (2011)
- [18] A.S. Ferlauto, G.M. Ferreira, J.M. Pearce, C.R. Wronski, R.W. Collins, X. Deng, G. Ganguly, *J. Appl. Phys.* 92, 2424 (2002)
- [19] J. Tauc, R. Grigorovici, A. Vancu, *Phys. Status Solidi (b)* (1966)
- [20] H. Lü, S. Wang, X. Wang, *J. Appl. Phys.* 115, 124107 (2014)
- [21] T. Zhang, W. Zhang, Y. Chen, J. Yin, *Opt Commun.* 281, 439 (2008)
- [22] F. Urbach, *Phys. Rev.* 92, 1324 (1953)
- [23] H.W. Martienssen, *J. Phys. Chem. Solids* 2, 257 (1957)
- [24] M.V. Kurik, *Phys. Statu Solidi (a)* 8, 9 (1971)

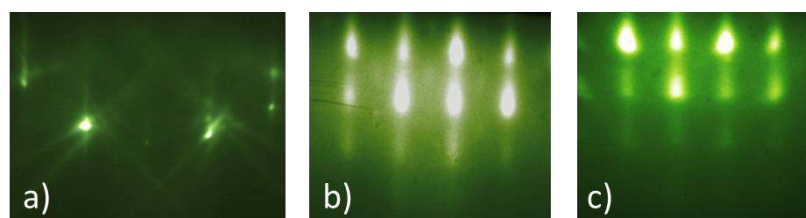


Figure 1: Typical RHEED patterns along the [100] direction for (a) the STO substrate, and (b) the NBT1 and (c) the NBT2 thin film samples

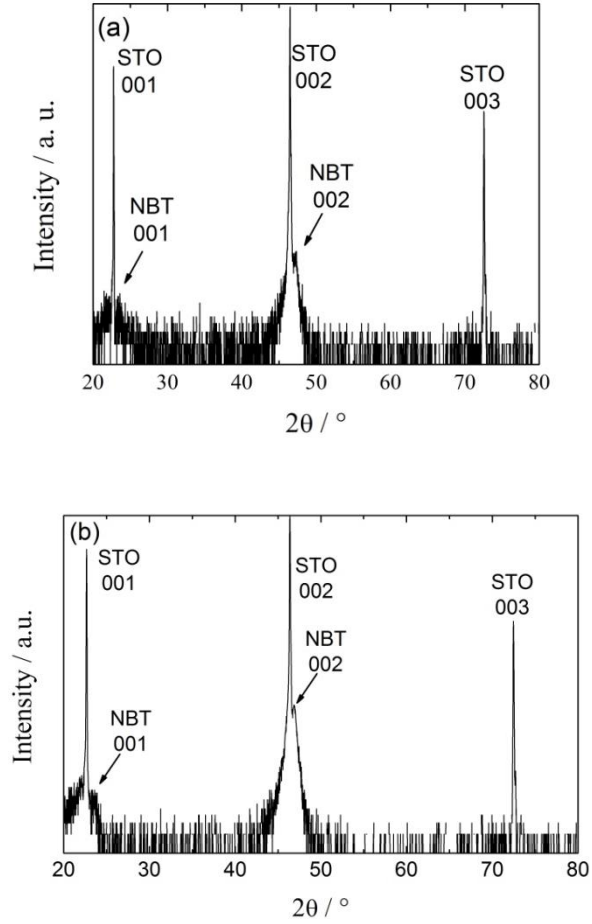


Figure 2: θ – 2θ X-ray diffraction (XRD) profiles of the NBT1 (a) and the NBT2 (b) samples. The intensity is plotted in logarithmic scale.

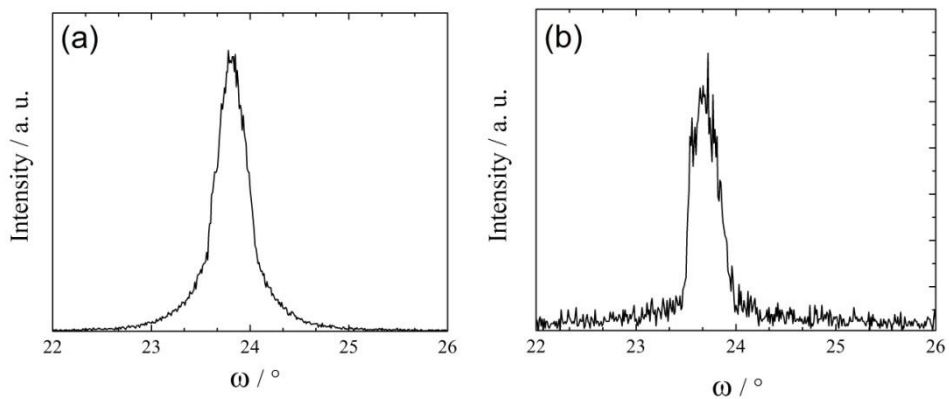


Figure 3: Comparison of the rocking curves of the two NBT thin films: NBT1 (a) and NBT2 (b). The rocking curve is recorded around the (002) reflexion.

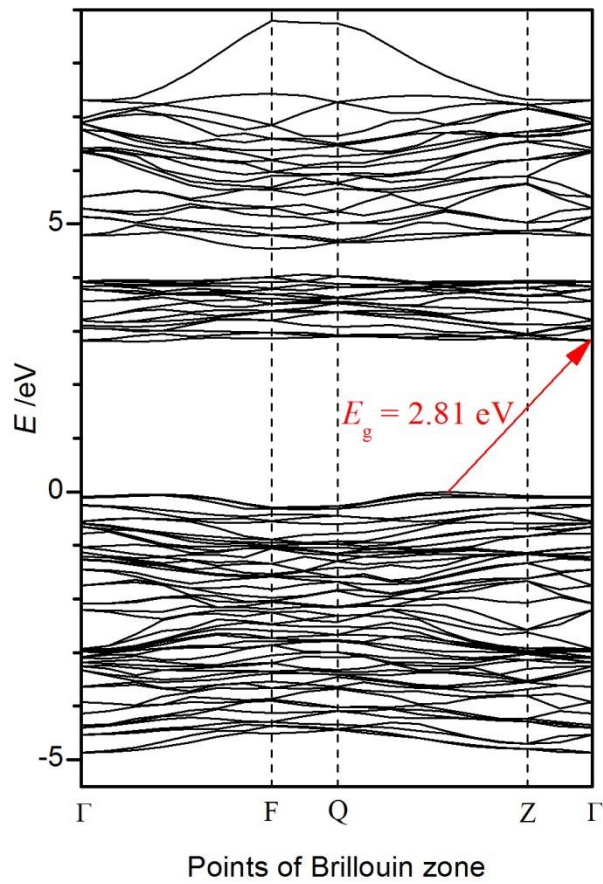


Figure 4: Electronic band structure of bulk NBT at the space group $R3$ (no. 146) for the points $\Gamma(0\ 0\ 0)$, $F(0\ 1/2\ 0)$, $Q(0\ 1/2\ 1/2)$, and $Z(0\ 0\ 1/2)$ of the Brillouin zone in the energy range -5.5 – 9.0 eV.

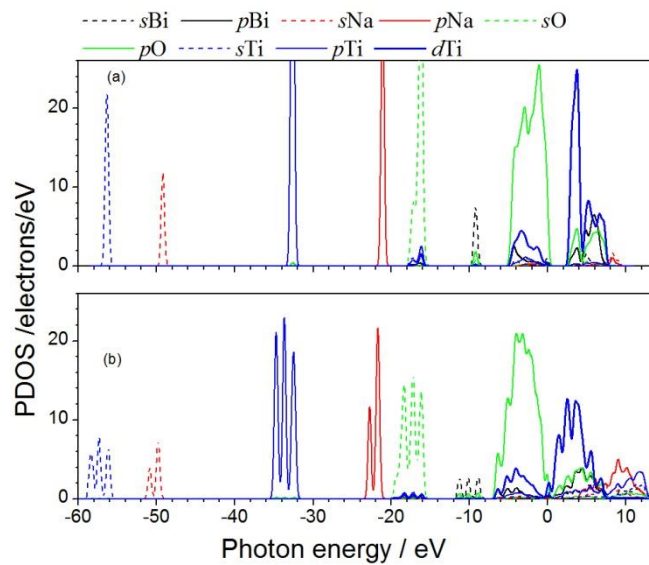


Figure 5: Partial density of states (PDOS) of the (a) bulk and (b) one-unit cell (001) slab of NBT.

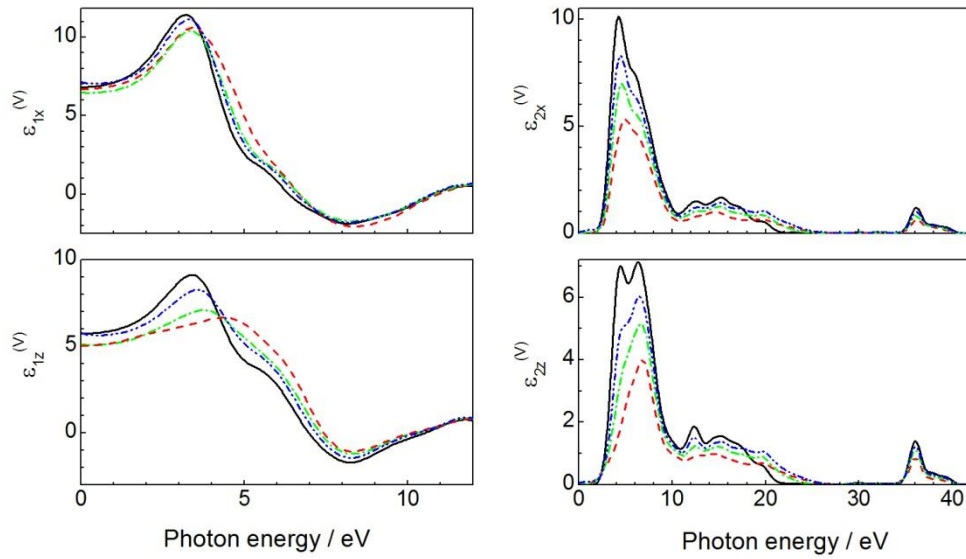


Figure 6: Real $\epsilon_1^{(V)}$ (left panels) and imaginary $\epsilon_2^{(V)}$ (right panels) parts of the dielectric functions for bulk NBT (black solid line), one (red dashed line), two (green dashed-dotted line) and four (blue dashed-dot-dotted line) unit cells NBT slabs.

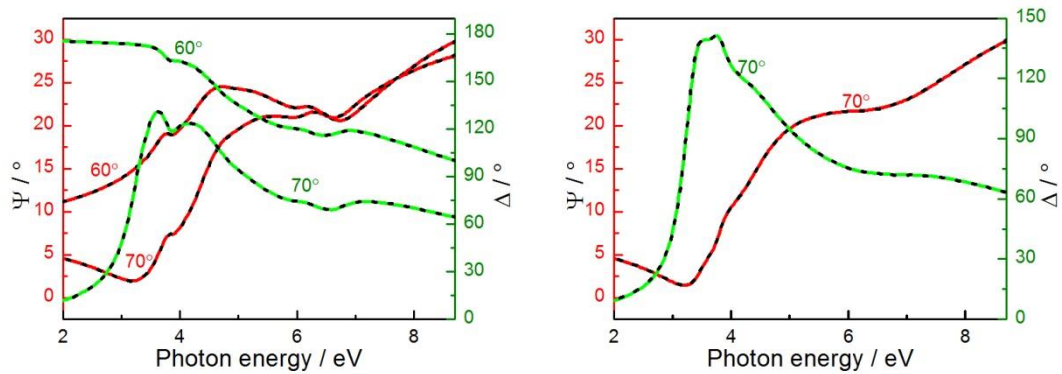


Figure 7: Experimental (dots) and simulated (lines) ellipsometric spectra $\Psi(E)$ (red), $\Delta(E)$ (green) for NBT1 (left panel) and NBT2 (right panel). Only spectra measured by the VUV-VASE instrument are shown for better clarity.

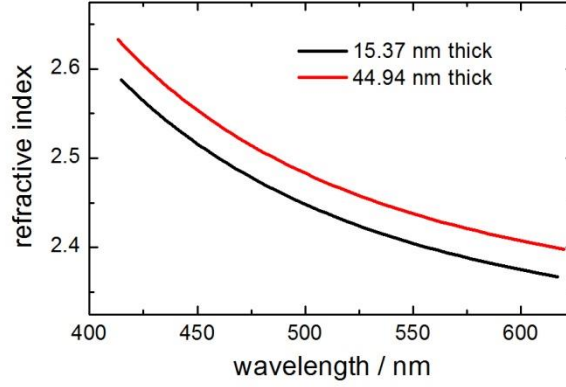


Figure 8: Dispersion of the refractive index for 15.37 nm and 44.94 nm thick NBT films obtained from the Cauchy model (Cauchy parameters A , B , C are equal to 2.27, 0.022, 0.005, respectively, for thinner, and analogous 2.30, 0.02, 0.006 for thicker film).

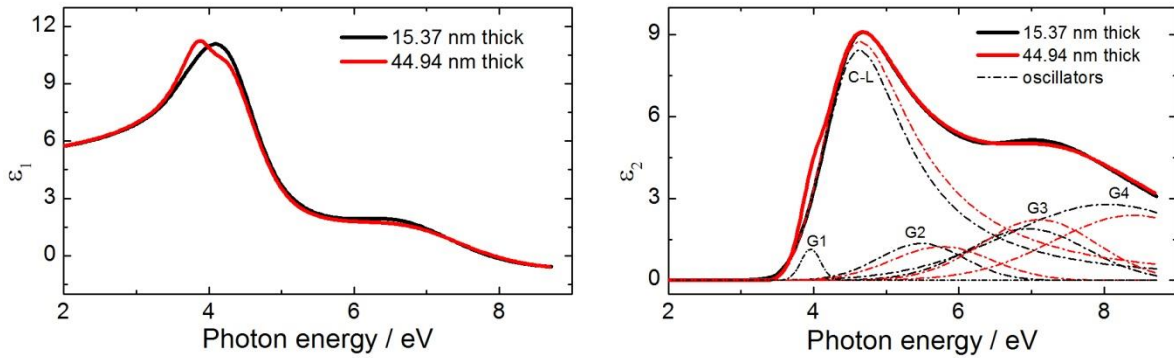


Figure 9: Real ϵ_1 and imaginary ϵ_2 part of the complex dielectric functions of both epitaxial (001)NBT thin films on STO. Dashed-dotted lines show the contributions of the individual oscillators to the entire $\epsilon_2(E)$ (solid lines).

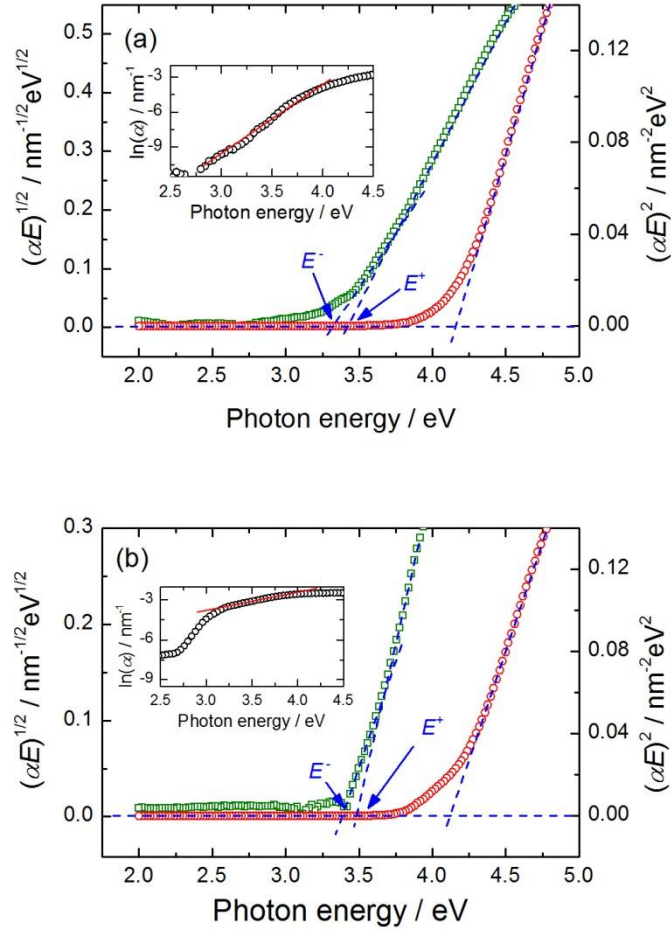


Figure 10. $(\alpha E)^{1/2}$ (green) and $(\alpha E)^2$ (red) as a function of the photon energy for (a) NBT1 and (b) NBT2. The inset shows $\ln(\alpha)$ vs. energy.

Table 1. Experimentally determined energies $E\#$ and amplitudes $A\#$ of the Gaussian oscillators

Sample	G1 / eV	A1	G2 / eV	A2	G3 / eV	A3	G4 / eV	A4
BNT130	-	-	5.48	1.35	6.95	1.88	8.05	2.78
BNT151	3.95	1.27	5.70	1.39	7.15	2.11	8.44	2.30

Table 2. Experimentally determined parameters of the Cody-Lorentz model: central peak position E_0 , energy gap E_g and the Urbach energy E_U .

Sample	E_0 / eV	E_g / eV	E_U / eV
BNT130	4.49	3.26	0.207
BNT151	4.40	3.34	0.200